Torque distribution influence on tractive efficiency and mobility of off-road wheeled vehicles

C. Senatore[a,1,*], C. Sandu[b,1]

[a]*Department of Engineering Science and Mechanics, Virginia Tech, Blacksburg, VA 24061, USA.*
[b]*Department of Mechanical Engineering, Virginia Tech, Blacksburg, VA 24061, USA.*

Abstract

Off-road vehicle performance is strongly influenced by the tire-terrain interaction mechanism. Soft soil reduces traction and significantly modifies vehicle handling; therefore tire dynamics plays a strong role in off-road mobility evaluation and needs to be addressed with ad-hoc models. Starting from a semi-empirical tire model based on Bekker-Wong theory, this paper, analyzes the performance of a large four wheeled vehicle driving on deformable terrain. A 14 degree of freedom vehicle model is implemented in order to investigate the influence of torque distribution on tractive efficiency through the simulation of front, rear, and all wheel drive configuration. Results show that optimal performance, regardless vertical load distribution, is achieved when torque is biased toward the rear axle. This suggests that it is possible to improve tractive efficiency without sacrificing traction and mobility. Vehicle motion is simulated over dry sand, moist loam, flat terrain and inclined terrain.

Keywords: tractive efficiency, off-road tire dynamics, multi-pass, vehicle dynamics, torque distribution

1. Introduction

The objective of this paper is to investigate the influence of torque distribution on tractive efficiency of wheeled off-road vehicles. Tires allow the vehicle to convert the energy delivered by the engine into useful work (motion) and therefore they influence vehicle dynamics and mobility. In order to realistically evaluate

*Corresponding author
Email addresses: themast@vt.edu (C. Senatore), csandu@vt.edu (C. Sandu)

the tractive efficiency of a full size vehicle it is necessary to properly model the dynamics of the tires and the vehicle body. For this reason a thorough off-road tire model is explained and a 14 degrees of freedom vehicle model is implemented.

Amongst the terramechanics community three primary approaches for tire-terrain interaction modeling can be summarized: semi-empirical methods [2, 31, 22, 12, 13], analytical methods [17, 30], and finite element methods [28, 29, 18]. In this paper, a the semi-empirical approach, based on work by Bekker [2], Reece and Wong [33, 34], is followed because semi-empirical models are computationally inexpensive and therefore they are suitable for real-time vehicle simulation. At the same time they allow to simulate tire complex behaviours such as slip-sinkage and multi-pass which significantly influence mobility and performance; as highlighted by Letherwood and Gunter [19] simplified tire models lead to poor prediction of vehicle dynamics and for this reason they are not suitable for this study. On the contrary, finite element analysis is still computationally demanding and it is not yet applicable for real-time simulations.

The simulation of an off-road vehicle differs from the on-road counterpart mainly for the tire-terrain interaction model. The dynamics of vehicle body is a well documented subject and extensively analyzed in the literature. To a good, first approximation, the vehicle can be modeled as a rigid body having six degrees of freedom [9, 10]. A vehicle model that incorporates a full scale off-road tire model has been proposed by Sharaf et al. [26, 25]. The authors adopted Harnisch et al. AS2TM tire model [14], performed standard handling maneuvers, and concluded that "in order to achieve the maximum tractive efficiency, the driving torque should be distributed to match the weight distribution between the front and rear axles in a manner as to minimize the slip difference between them".

Yamakawa et al. [35] studied independent wheel drive vehicles and highlighted in their conclusions that "torque allocation based on the vertical load on the individual wheels is one possible method for efficiently controlling wheel torque for vehicles with independently driven wheels".

In this paper we show that load distribution does not have a strong impact on tractive efficiency (it influences mobility though) and that, due to different tire-soil characteristic between front and rear axle (multi-pass), slip minimization does not necessarily guarantee optimal traction, but we will show that it remains intimately related.

The paper is structured as follows: section 2 explains the tire model, section 3 introduces the full vehicle model and section 4 presents the results.

2. Tire Model and Assumptions

The adopted model has been developed by the authors in [24], thus it will only be briefly introduced here. The model accounts for both rigid wheels and flexible tires. The rigid wheel implementation is substantially based on the model developed by Wong and Reece [33, 34] while the flexible tire implementation follows the approach proposed by Chan and Sandu [4, 6, 5]. Key features of this model are the inclusion of multi-pass effect and slip-sinkage phenomenon for both rigid and flexible wheels. Rigid wheels can be considered a first approximation of a flexible tires. When the terrain stiffness is significantly lower than the total tire stiffness (the carcass stiffness plus the inflation pressure), the flexible tire can be approximated as a rigid wheel, greatly simplifying the analysis.

The first step for a semi-empirical method is to estimate the stress distribution along the contact patch. Normal and shear stresses develop at the interface between a rotating tire and the soil surface. Normal stress is calculated from the pressure-sinkage equation originally introduced by Bekker [1] and later modified by Reece (1),

$$\sigma_n = (ck'_c + b\gamma_s k'_\phi)\left(\frac{z}{b}\right)^n, \tag{1}$$

where σ_n is the pressure normal to the sinkage plate, z is the sinkage, n is called sinkage index, c is the soil cohesion,γ_s is the soil bulk density, k'_c is a cohesion-dependent soil coefficient, k'_ϕ is a frictional-dependent soil coefficient, and b is a parameter related to the geometry of the penetrometer (the radius for circular plates or the smaller linear dimension for rectangular plates).

Calculation of the shear stress beneath the wheel is based upon an empirical expression first introduced by Janosi and Hanamoto [16] and widely used,

$$\tau_x = (c + \sigma_n \tan\phi)\left(1 - e^{\frac{-j_x}{k_x}}\right), \tag{2}$$

where the first term is the Mohr-Coulomb failure criterion and represents the limiting shear stress (ϕ is the angle of internal friction of the material), j_x is the shear displacement of the terrain, and k_x is the shear deformation modulus (a measure of displacement needed to achieve maximum shear stress). Shear properties of soil c, ϕ, and k_x can be obtained though direct shear tests or ring shear tests. Norm Shear displacement j_x describes the relative velocity between the wheel and terrain at the interface. It can be calculated integrating the shear velocity of the soil in contact with the wheel (assuming that the velocity of terrain particles at the interface

matches the velocity of the tire). According to Wong [33], it can be defined as follows:

$$j_x = \int_{\theta_b}^{\theta_e} R_{eff}(\theta)[1-(1-s_d)\cos(\theta)]\,d\theta \tag{3}$$

j_x, as well as σ_n and τ, are function of the central angle θ which is illustrated in figure 2. R_{eff} is the effective radius and it will be discussed in detail later in this section while s_d is the slip ratio and it is defined as follows:

$$s_d = 1 - \frac{V}{\omega R_l} \tag{4}$$

where V is the velocity of the axle of the wheel it the x'-direction (defined in section 3), ω is the angular velocity of the wheel, and R_l is the rolling radius. In order to reproduce a realistic stress distribution, normal stress is defined in this study as a piecewise function [33]. From leading edge θ_e to the location of the maximum normal stress, θ_m, the stress is calculated using (5),

$$\sigma_{nf}(\theta) = (ck'_c + b\gamma_s k'_\phi)\left(\frac{R_{eff}}{b}\right)^n (\cos(\theta)-\cos(\theta_e))^n, \tag{5}$$

while the normal stress that goes from the maximum stress point, θ_m, to the trailing edge, θ_b, can be evaluated by (6),

$$\sigma_{nr}(\theta) = (ck'_c + b\gamma_s k'_\phi)\left(\frac{R_{eff}}{b}\right)^n \left(\cos\left(\theta_e - \left(\frac{\theta-\theta_r}{\theta_m-\theta_r}\right)(\theta_e-\theta_m)\right)-\cos(\theta_e)\right)^n. \tag{6}$$

Typical trend of normal and tangential stress distribution are given in figure 1. In this study, θ_m is thought to be a linear function of the slip ratio and the entry angle. This is an empirical estimation successfully implemented in other studies [33, 27, 20].

$$\theta_m = (c_0 + c_1|s_d|)\theta_e, \tag{7}$$

c_0 and c_1 are two constants. Since θ_m is usually half-way between the entry angle and exit angle, c_0 can be selected in the range of $[0.4, 0.5]$ and $c_1 \in [0.2, 0.4]$ as proposed by [33]. It should be mentioned that Wong has suggested a different definition of θ_m for negative slip: however such definition creates discontinuity issues around zero slip and thus it was not considered here also because no breaking maneuver are simulated. To improve the prediction of slip-sinkage the sinkage exponent n is linearly related to the slip ratio [20].

$$n = n_0 + n_1 |s_d| \tag{8}$$

This is again an empirical approximation but it contains some physical insight. The exponent n is experimentally obtained for steady soil loading tests performed with a bevameter. However, the response of the soil in contact with a rolling/slipping tire is presumably different. Thus, equation (8) is introduced to describe the variation of sinkage exponent as a function of wheel slip. In this work constants n_0 and n_1, experimentally obtained thorough single wheel drawbar tests by [20], have been adopted.

A tire operating on deformable soil can be approximated as a rigid wheel if the pressure distribution along the contact patch does not exceed the carcass stiffness. When this is verified the effective radius is a constant, and it equals the undeformed radius, $R_{eff} = R_u$. When carcass stiffness is exceeded, the tire deforms and a different approach is needed. The problem becomes extremely complex because both the tire and the terrain are deformable. Chan and Sandu proposed to calculate the deflected shape of the tire through the following equation:

$$R_{eff} = \begin{cases} R_u - R_u \left(1 - \frac{1-\frac{\delta}{R_u}}{\cos(\theta)}\right) & \text{if } \theta_r < \theta \leq \theta_f \\ R_u - R_u \left(1 - \frac{1-\frac{\delta}{R_u}}{\cos(\theta_f)}\right) e^{-\beta\left(\sqrt{1+\zeta^2}+\zeta\right)(\theta-\theta_f)} & \text{if } \theta_f < \theta \leq \pi \\ R_u - R_u \left(1 - \frac{1-\frac{\delta}{R_u}}{\cos(2\pi+\theta_r)}\right) e^{\beta\left(\sqrt{1+\zeta^2}-\zeta\right)(\theta-(2\pi+\theta_r)} & \text{if } \pi < \theta \leq 2\pi+\theta_r \end{cases} \tag{9}$$

ζ and β are two parameters related to the stiffness, damping, size, inflation pressure, angular velocity and construction of the tire and are obtained experimentally [4, 21, 36, 11]. An example of a deformed tire is given in figure 2. The tire has a flat shape between the angles θ_f and θ_r and a round shape (connected through a logarithm spiral) elsewhere.

2.1. Multi-Pass Effect

Multi-pass effect has a strong impact on the evaluation of traction of off-road vehicles. Repetitive loading of deformable soils showed that during the unloading and reloading process the pressure-sinkage relation can be approximated with a straight line [31]. However, the modeling of repetitive loading introduced by Wong cannot be directly implemented into the model because of the way the normal stress along the contact patch have been obtained (a piecewise function that

does not strictly follow the monotonic trend of the sinkage). In this paper a different approach is taken. The most relevant study concerning the multiple pass of wheels on the same patch of terrain is the one performed by Holm [15]. The study showed that terrain properties are altered after each pass and the variations are a function of slip. If the first wheel is towed (zero torque pass), soil properties vary mildly, while the passage of a slipping tire produces a stronger effect. Holm's results are reproduced in figure 3 where the experimental results are fitted through the following equation:

$$\gamma_{sn} = \gamma_s \left[1 + \left(1 - e^{\frac{-s_0}{k_1}} \right) k_2 + k_3 n_p \right], \tag{10}$$

where k_1, k_2, k_3, are three fitting constants that can be derived from experiments while s_0 is the slip of the previous pass and n_p is the number of passes. The greatest variation occurs between the first and second pass: successive runs have less impact on the behavior of the terrain. Terrain density increases after each pass and, considering the obtained results and related work from Bekker [3], also the cohesion of the material is considered to have increased. This phenomenon is incorporated into the model introducing a dependency of soil properties c, and k_x upon the number and type of passes through the following equations:

$$c_n = c \left[1 + \left(1 - e^{\frac{-s_0}{k_1}} \right) k_2 + k_3 n_p \right], \tag{11}$$

$$k_{xn} = k_x \left[1 - \left(1 - e^{\frac{-s_0}{k_1}} \right) k_2 - k_3 n_p \right]. \tag{12}$$

We speculate that c and k_x follow the same trend as in equation (10); thus, k_1, k_2, k_3 have the same value in equations (10),(11),(12). Extrapolated parameters, employed in this study, are presented in table 3.

2.2. Drawbar Pull, Driving Torque, and Lateral Force

Once the normal and tangential stress distributions are known it is possible to calculate the drawbar pull and the driving torque. The balance of vertical forces needs to be calculated first: it ensures that the vertical force produced along the contact patch balances the vertical load acting on the wheel, as given in (13),

$$W = w \int_{\theta_b}^{\theta_e} R_{eff}(\theta) \left(\sigma_n(\theta) \cos(\theta_{eff}) + \tau_x(\theta) \sin(\theta_{eff}) \right) d\theta, \tag{13}$$

Table 1: Undisturbed soil properties adapted from [32] simulations. Moisture content is zero for dry sand and about 50% for moist loam.

Soil	k'_c	k'_{phi}	n	c [Pa]	ϕ [deg]	k_x,k_y [m]	γ_s [N/m^3]
Dry Sand	34	49.68	0.70	1150	31.1	0.015	15,696
Moist Loam	24.45	96.34	0.97	3300	33.7	0.0076	15,196

where W is the weight force of the vehicle and the right hand side term represents the integrated stress along the contact patch acting in the vertical direction (i.e., the vertical force exerted by the tire). The tire width is w while θ_{eff} is the effective angle that the deformed tire shape creates with the vertical axis; for the rigid wheel model θ_{eff} is equal to θ. Drawbar pull F_x is calculated from the integration of the normal and shear stresses decomposed along the longitudinal direction,

$$F_x = w \int_{\theta_b}^{\theta_e} R_{eff}(\theta) \left(\tau_x(\theta) \cos(\theta_{eff}) - \sigma_n(\theta) \sin(\theta_{eff}) \right) d\theta. \tag{14}$$

It should be mentioned that this expression already includes the soil compaction resistance, given by the last term of the integral.

The driving torque is given by the following expression:

$$T = w \int_{\theta_b}^{\theta_e} R_{eff}^2(\theta) \tau_x(\theta) d\theta. \tag{15}$$

The tire model has been tested on two type of terrain: dry sand and moist loam. Dry sand is a non-cohesive and loose soil; on such terrain the carcass stiffness is never exceeded and the tire operates as a rigid wheel. Loam is a firmer soil which exhibits a steeper pressure-sinkage curve; on this terrain both the soil and the tire deforms. Soil and tire properties are summarized in Tables 1, 2.

Table 2: Nominal tire properties needed to calculate tire geometry according to equation 9. Parameters are referred to a Continental Contitrac SUV P265/70/R17 and have been experimentally calculated in [4].

R_u [m]	w [m]	p_i [kPa]	ζ	β	δ
0.4	0.265	240	0.0845	6.3579	0.0230

Table 3: Tire parameters for slip-sinkage and multi-pass calculation. c_0 and c_1 are taken from [33]. c_{0f} and c_{1f} are estimated by inspection. n_0 and n_1 are taken from [20]. k_1, k_2, and k_3 are extrapolated form [15] as explained in the text. All parameters are dimensionless.

c_0	c_1	c_{0f}	c_{1f}	n_0	n_1	k_1	k_2	k_3
0.4	0.2	0.2	0.05	0.8	0.6	0.1178	0.1672	0.0348

2.3. Tire Response

In this section a concise overview of tire model features is presented. Figure 4 shows the trend of the drawbar pull and torque versus the slip ratio at different vertical loads on dry sand (tire behaves as a rigid wheel). Longitudinal force is much higher (in absolute value) for negative slip because of the sinkage phenomenon: terrain compaction force always acts against the direction of travel.

The multi-pass effect can radically change the performance of tires rolling into ruts created by other tires of the same or other vehicles. Figure 5 shows the variations of drawbar pull and sinkage for multiple passages predicted by the tire model. As mentioned previously the way the first pass is performed affects the terrain properties and the performance of the second pass. This has direct implications for multi-axle vehicles where only some of the axles are driven. The drawbar pull increases at the successive passages while the relative sinkage decreases because of terrain compaction.

Similar results are obtained on moist loam and are omitted here because of space limitations. A more exhaustive description is given in [24]

2.4. Traction Efficiency

The resistance to motion at tire-soil interface is predominantly influenced by the terrain compaction that results from sinkage. A measure of the efficiency, according to Wong [31], can be obtained comparing the thrust power with the driving power:

$$\eta_t = \frac{F_x v_x}{T\omega} = \frac{F_x(1-s_d)R_l}{T}. \tag{16}$$

Tractive efficiency depends upon the slip s_d and the effective rolling radius R_l and it provides a measure of the capability to convert the power delivered to the wheels into actual motion (the effective rolling radius is either the undeformed radius R_u for rigid wheels or $\min(R_{eff})$ for flexible tires).

Tractive efficiency can be split into two terms: efficiency of motion,

$$\eta_m = \frac{F_x R_l}{T}, \tag{17}$$

and efficiency of slip,

$$\eta_s = 1 - s_d. \tag{18}$$

The efficiency of motion is a direct measure of the ability to convert the applied torque into useful drawbar pull. The efficiency of slip measures the losses due to slip effect. For a four wheel drive vehicle, assuming same performance of the two front and rear tires, it is possible to express the slip efficiency as follows:

$$\eta_s = 1 - \frac{s_{df} u_f F_f + s_{dr} u_r F_r}{u_f F_f + u_r F_r}. \tag{19}$$

where the indexes f and r refer to the front and rear axle respectively. Introducing the ratio of theoretical speed,

$$K_v = \frac{u_f}{u_r} = \frac{1 - s_{dr}}{1 - s_{df}}, \tag{20}$$

and the coefficient of thrust distribution,

$$K_d = \frac{F_r}{F_f + F_r}, \tag{21}$$

and through some mathematical manipulations it is possible to express the slip efficiency for a four wheel drive vehicle as follows:

$$\eta_s = 1 - \frac{s_{df}(1 - s_{dr}) - (s_{df} - s_{dr})K_d}{(1 - s_{dr}) - (s_{df} - s_{dr})K_d}. \tag{22}$$

Setting the first partial derivative of equation (22) with respect to K_d equal to zero it is possible to find the optimal slip distribution:

$$\frac{\partial \eta_s}{\partial K_d} = \frac{(1 - s_{df})(1 - s_{dr})(s_{df} - s_{dr})}{\left[(1 - s_{dr}) - (s_{df} - s_{dr})K_d\right]^2} = 0 \tag{23}$$

Equation (23) is satisfied when s_{df} and s_{dr} are both equal to 1 (100% slip) and when $s_{sd} = s_{dr}$. Clearly the first possibility corresponds to zero efficiency because if both axles have 100% of slip the vehicle cannot move. The slip efficiency is maximized when the slip difference between the front and the rear axle is minimized. This theoretical results holds if front and rear tires behaves in the same

way. However, besides of the possibility of different wear and inflation pressure, rear tires hardly behave like front tires because of the multi-pass effect. In section 4 we will show that optimal torque distribution does not always correspond to the condition that minimizes slip difference. Multi-pass effect intrinsically enhances the efficiency. This is expected because firmer soil reduces sinkage and provides better traction. The increase of vertical load (due to increased vehicle weight or load transfer phenomena during motion) has a marginal negative effect: higher values of F_z enhance traction but at the same time increase sinkage (i.e., compaction resistance) and deteriorate efficiency.

Figures 6,7 present tractive efficiency for tires rolling on dry sand (rigid) and loam (flexible) terrain. Tractive efficiency increases for larger tires, lower inflation pressure and successive passes. This happens because in these conditions sinkage decreases leading to a reduced compaction resistance force. During on-road operations higher inflation pressure guarantees better fuel economy but this is not the case in off-road. Reduced inflation pressure not only improves traction but it also reduces sinkage, which also improves efficiency (hysteresis losses are negligible if compared with terrain compaction losses). On loamy soil, the increase in vertical load has a stronger impact than that showed by dry sand. This is due to the fact that loam is a firmer soil and the compaction resistance due to sinkage is more significant.

The efficiency, for both soils, has a peak in the range of 10-20% slip. It should be remembered that it is not possible to force the tires to work at an imposed slip ratio (the slip is indirectly controlled by the driver through the control of the desired vehicle speed). What can be done is to properly match the tires, the powertrain ratio and the torque distribution in order to optimize the motion in specific working conditions.

3. Vehicle Model

A full vehicle model is implemented and integrated with the tire model. To limit simulation complexity some simplifications are introduced: vehicle body flexibility is not considered, steering mechanism is modeled only in its kinematics, inertia properties of the drive-line are not considered, no camber or toe angle is considered, suspensions' kinematics is linear.

3.1. Equations of Motion

The vehicle model is based on the analysis discussed in [9, 8, 7, 26]. Figure 8 presents the vehicle model scheme. Five masses are considered:

- the vehicle sprung mass m_s, concentrated at the center of gravity of the body,
- four unsprung masses m_u located at the center of the wheel hubs. These masses account for the rims, the tires, and suspension assemblies.

Three reference frames are defined following the recommendations of SAE J670e [23]:

- the inertial reference frame X,Y,Z: a right-handed earth-fixed coordinate system
- the vehicle reference frame x,y,z: a right-handed vehicle-fixed coordinate system attached to the sprung mass. The origin is located at the center of gravity (CG) of the sprung mass.
- the tire reference frame x',y',z': four right-handed tire-fixed coordinate systems attached to the unsprung masses. The z'-direction is always parallel to the vehicle-fixed z-direction. Directions x' and y' are parallel to x and y only for the rear wheels (which are not steered). The suffixes fl, fr, rl, rr will be used to refer respectively to: front-left, front-right, rear-left and rear-right (intended for an observer that is sitting in the car, facing the positive direction of the x-axis in the vehicle-fixed reference frame).

The sprung mass is modeled as a 6 degree of freedom (DOF) rigid body. The wheels are connected to the vehicle body via springs and dampers. No relative motion in the x and y directions between the wheels and the car body is assumed. The tire displacement is constrained in the z vehicle-fixed direction only. However, the wheels have an extra degree of freedom represented by the angular velocity. The non-linear and unsteady sprung mass motion can be described by the Newton-Euler equations, written with respect to the vehicle-fixed reference frame. This choice guarantees a straight forward calculation of the external forces acting on the body. The equations of motion can be written as follow [8]:

$$\begin{aligned}
\sum F_x &= ms(\dot{u}+wq-vr)\\
\sum F_y &= ms(\dot{v}+ur-wp)\\
\sum F_z &= ms(\dot{w}+vp-uq)\\
\sum M_x &= \dot{L}_x+qL_z-rL_y\\
\sum M_y &= \dot{L}_y+rL_x-pL_z\\
\sum M_z &= \dot{L}_z+pL_y-qL_x,
\end{aligned} \tag{24}$$

where:

u, v, w = vehicle-fixed components of the sprung mass linear velocity,

p, q, r = vehicle-fixed components of the sprung mass angular velocity,

F_x, F_y, F_z = vehicle-fixed components of external and internal forces,

M_x, M_y, M_z = vehicle-fixed components of external and internal moments,

L_x, L_y, L_z = vehicle-fixed components of angular momentum.

The unsprung masses are modeled with a quarter car model. As previously stated the motion of the wheels is constrained to the z-direction in the vehicle-fixed reference frame. The dynamics of the unsprung masses can be modeled as follow:

$$\begin{aligned} m_u \ddot{z}'_{fl} &= F_{sfl} + k_t(z'_{tfl} - z'_{fl}) \\ m_u \ddot{z}'_{fr} &= F_{sfr} + k_t(z'_{tfr} - z'_{fr}) \\ m_u \ddot{z}'_{rl} &= F_{srl} + k_t(z'_{trl} - z'_{rl}) \\ m_u \ddot{z}'_{rr} &= F_{srr} + k_t(z'_{trr} - z'_{rr}), \end{aligned} \tag{25}$$

where:

$z'_{fl}, z'_{fr}, z'_{rl}, z'_{rr}$ = tires vertical displacement,

$F_{sfl}, F_{sfr}, F_{srl}, F_{srr}$ = suspension forces,

k_t = tire stiffness,

$z'_{tfl}, z'_{tfr}, z'_{trl}, z'_{trr}$ = terrain vertical displacement.

The calculation of the roll, pitch, and yaw angles (Euler angles) requires the integration of the angular velocity components p, q, r through the kinematic differential equation (26). It should be recalled that direct integration of the angular velocity components yields erroneous results. The correct approach integrates the angular velocity components along the axes of rotation of the Euler angles. In this study the order of rotations chosen is yaw, pitch, roll:

$$\begin{aligned} \dot{\phi} &= p + (q\sin\phi + r\cos\phi)\tan\theta \\ \dot{\theta} &= q\cos\phi - r\sin\phi \\ \dot{\psi} &= (q\sin\phi + r\cos\phi)\sec\theta \end{aligned} \tag{26}$$

The presence of $\tan\theta$ and $\sec\theta$ introduces a singularity when the pitch angle equals $\frac{\pi}{2}$. This problem can be avoided with introducing the quaternions or an indexing scheme. However, no countermeasure is taken because the pitch angle will remain small during motion.

The external forces acting on the vehicle are:

- forces and moments generated at the tire-terrain contact patches,
- aerodynamic force (only in the x-direction),
- gravitational force,

The internal forces are:

- forces produced by the springs compression/extension,
- forces produced by the dampers compression/extension.

A proportional integral (PI) controller is introduced to maintain the imposed cruise speed. The error function ε depends on the difference between the target velocity V_{set} and the longitudinal velocity u:

$$\varepsilon(t) = V_{set} - u(t), \tag{27}$$

where the notation explicitly includes the time dependence. The controller acts on the torque delivered to the wheels through the following equation:

$$T(t) = K_p\varepsilon(t) + K_i\int_0^t \varepsilon(\tau)d\tau \tag{28}$$

where:

K_p = proportional gain,

K_i = integral gain.

3.2. Torque Distribution

For front (rear) wheel drive vehicles torque is equally divided between left and right wheel of the axle, in this case no torque is delivered to the rear (front) axle. Non driven wheels will receive zero torque but will produce a negative force because of the terrain compaction resistance that still acts on them. Front (rear) wheel drive vehicles will be labeled FWD (RWD) while all/four wheel drive vehicles will be labeled AWD.

In the case of four wheel drive vehicles torque will be distributed equally among left and right wheel (the axle differentials always split the torque equally). On the other hand, torque distribution among the front and rear axles (governed by the central differential) will be varied.

The adopted vehicle parameters represent typical values for a large SUV and are summarized in Table 4.

Table 4: Vehicle specifications.

m_s = 2500 kg	m_u = 44 kg
J_x = 1165 kgm^2	c_f = 2700 Ns/m
J_y = 5348 kgm^2	c_r = 3300 Ns/m
J_z = 5721 kgm^2	k_f = 25 kN/m
a = 1.48 m	k_r = 21 kN/m
b = 1.52 m	ρ = 1.28 kg/m^3
L = 3 m	S_c = 2.44 m^2
B = 1.7 m	k_t = 270395 kN/m

4. Results

Hitherto, the tire model and the vehicle model have been developed and explained separately. In this section the results for a full-vehicle, and adopting the tire model developed in Section 2, are presented. Since the tire model has been developed under steady state assumptions, the full-vehicle simulation is performed at constant longitudinal speed. The simulations are started at a velocity slightly lower than the target one, and the PI controller equation (28) is used to reach smoothly the cruise speed. The efficiency is analyzed when steady state conditions are reached. The transients have to be regarded as a first approximation of the vehicle dynamics.

4.1. Dry Sand

Figure 9 shows the velocity profile and the applied torque, for a vehicle that starts at 20 km/h and has to reach the target speed of 25 km/h. FWD, RWD and AWD configurations are plotted together: in every configuration the vehicle is able to reach the imposed speed. The PI controller adjusts the torque correctly in order to reach the target speed.

Similar plots are obtained for the other variables of interest but are omitted here for the sake of brevity.

2WD vehicles have the handicap of dragging a non-driven axle: free rolling wheels, sink into the terrain and produce a negative force due to the terrain compaction. This causes the front (rear) wheels of the AWD (RWD) vehicle to slip significantly in order to produce the desired level of longitudinal force. Increased slip means increased sinkage and consequently poorer efficiency. The AWD vehicles, distributing the torque evenly between the front and rear axle, have more balanced performance. Traction efficiency is primarily influenced by sinkage. Rear wheels are always sinking less (relatively) than front wheels allowing for better traction performance at the rear axle. Even for vehicles driving uphill (where load transfer can be in the order of 10-15%), increased vertical load on rear wheels does not compensate for soil stiffening behavior: back wheels sink less than front ones. Sinkage difference between axles, depending on simulation scenarios, varies from 1 cm up to 4 cm.

The influence of torque distribution on the tractive efficiency has been studied varying the torque ratio among the front and rear axle. Figure 10 presents the power requirement for a full range of transmission configurations. In this plot 0 % means that all the available torque is delivered to the front axle (i.e., FWD vehicle,) while 100 % means that the rear axle receives full torque (i.e., RWD vehicle). For a vehicle traveling at 25 km/h there is a minimum in the vicinity of 50 %. Similar trend has been observed for higher velocities. Distributing the torque slightly toward the rear axle can improve the efficiency of the vehicle without sacrificing the performance. On the same plot also the slip difference ΔS_d between front and rear axle is plotted. In this particular configuration power minimum and slip differential minimum are very close.

The same analysis has been performed on a vehicle climbing a constant slope of 10 % inclination. In this scenario pure front wheel drive or rear wheel drive vehicles can't easily maintain a speed of 25 km/h. Figure 11 present the power vs torque distribution trend for this scenario. The trend is similar to the results obtained for flat terrain operations: the best efficiency is obtained when the torque

is biased toward the rear axle. Results for FWD and RWD vehicles are not presented because this drive configuration failed to complete the course (not enough traction).

Results for torque distribution presented in figures 10, 11 suggest that delivering more torque to the rear axle can improve tractive performance. It should be noted that in both cases weight transfer phenomena toward rear axle occurred (extremely moderate on flat terrain and in the order of 10-15 % for uphill scenario). In order to understand the influence of vertical load, a simulation of a vehicle significantly loaded on the front axle (i.e., CG translated closer to the front axle) have been performed. The results, presented in figure 12, show that torque distribution is moderately influenced by static load distribution: the optimum is still close to the 50% F - 50% R ratio and, in spite of a significant vertical load unbalance, has only marginally moved toward the front axle.

4.2. Moist Loam

This section analyzes the motion and the efficiency of a vehicle traveling on a straight line on moist loam. The loam is a cohesive soil and the tire will always perform as a flexible tire in this section.

Figure 13 presents the power requirement for a full range of transmission configurations on flat terrain. Also in this case a moderate shift of torque toward the rear axle guarantees better efficiency.

Another test is run on a 10% slope while the vehicle speed is set to 50 km/h. Figure 14(a) presents the power vs torque distribution trend for this scenario. The trend is similar to flat terrain operations: a minimum of power is observed for the the situation of torque biased toward the rear. It should be noted that on moist loam the variation of power is less significant. Results for pure FWD or pure RWD configurations (respectively 0% and 100% on the x-axis) are not presented because these vehicles were not able to travel at the desired speed.

The tire pressure has been decreased in order to investigate its influence on the efficiency of the vehicle. In this operational conditions the resistance force due to terrain compaction decreases consistently and this improves the performance. Figure 14(b) shows the instantaneous power requirement for a large range of torque distribution. The best efficiency is reached when the torque is biased to the rear axle. Under-inflated tires provide better efficiency on off road terrain, the power requirement is about 10% less then normally inflated tires.

5. Conclusions

In this paper a tool for predicting mobility, handling, and tractive efficiency of off-road vehicles is presented. A semi-empirical off-road tire model, based on the work of Wong and Reece [33, 34], and Chan and Sandu [4], has been implemented. The model is able to predict salient features encountered in off-road operations: slip-sinkage behavior and multi-pass effect have been modeled through the introduction of semi-empirical equations. The response of the model has been extensively investigated in order to verify the influence of several parameters. Variations of vertical load, tire geometry, tire inflation pressure, and soil states (i.e., multi-pass) showed that the model consistently predict tire tractive performance.

It has been shown that the proposed tire-model can be successfully adopted to simulate the large motion of an off-road vehicle. An analysis of the the tractive performance has been conducted. It has been shown that it is possible to improve the efficiency of off-road vehicles acting on the torque distribution of the vehicle. Shifting the torque toward the rear axle can help to exploit in a better way the tractive resources of the vehicle and obtain an improvement of the efficiency, without sacrificing the performance. This result has been obtained analyzing the vehicle with a high level of detail. The study highlighted that the motion of a vehicle can be optimized acting on torque distribution. It should be remembered that varying parameters such as tire size, static weight balance, and torque distribution can significantly modify the response of the vehicle. This can have implications on the safety and comfort.

Static load distribution influences traction but does not have a significant impact on tractive efficiency: the best tractive efficiency, under a large range of operational conditions, is reached when the torque distribution is biased toward the rear axle. This operational condition helps to optimize the slip efficiency which dominantly influences the overall tractive efficiency.

Acknowledgments

This work has been partially supported by the Automotive Research Center, through Thrust Area # 1 grant no. F017721, and by the National Science Foundation through the NSF GOALI award no. CMMI-0700278.

Bibliography

[1] M. G. Bekker. *Theory of Land Locomotion; the mechanics of vehicle mobility*. The University of Michigan Press, Ann Arbor, 1956.

[2] M. G. Bekker. *Off-The-Road Locomotion; research and development in terramechanics*. The University of Michigan Press, Ann Arbor, 1960.

[3] M. G. Bekker. *Introduction to Terrain-Vehicle Systems*. The University of Michigan Press, Ann Arbor, 1969.

[4] B. J. Chan. *Development of an off-road capable tire model for vehicle dynamics simulations*. PhD thesis, Virginia Polytechnic Institute and State University, Blacksburg, VA, 2008.

[5] B. J. Chan and C. Sandu. A novel wheel-soil interaction model for off-road vehicle dynamics simulation. In *Proceedings of ASME IDETC, 9th Int. Conf. on AVTT*, Sept. 4-7, Las Vegas, NV, 2007.

[6] B. J. Chan and C. Sandu. A semi-analytical approach to off-road tire modeling for vehicle dynamics simulations. In *Proceedings of 16th ISTVS International Conference*, Turin, Italy, 2008.

[7] T. D. Day, S. G. Roberts, and A. R. York. SIMON: A new vehicle simulation model for vehicle design and safety research. *SAE International*, (2001-01-0503), 2001.

[8] B. Etkin. *he Dynamics of Flight, Stability and Control*. John Wiley & Sons, New York, NY, 3rd edition, 1995.

[9] G. Genta. *Motor vehicle dynamics : modeling and simulation*. World Scientific, Singapore, 1997.

[10] T. D. Gillespie. *Fundamentals of vehicle dynamics*. Society of Automotive Engineers, Warrendale, PA, 1992.

[11] S. Gong. *A Study of in-plane Dynamics of Tires*. PhD thesis, T.U. Delft, Delft, Netherlands, 1993.

[12] A. Grečenko. Slip and drift of the wheel with tyre on soft ground. In *Proceedings of 3rd ISTVS International Conference*, volume II, pages 76–95, Essen, Germany, 1969.

[13] A. Grečenko. The slip and drift model of a wheel with tyre compared to some other attempts in this field. *Journal of Terramechanics*, 29(6):599–604, 1992.

[14] C. Harnisch, B. Lach, R. Jakobs, M. Troulis, and O. Nehls. A new tyre-soil interaction model for vehicle simulation on deformable ground. *Vehicle System Dynamics*, 43(Supplement):384–394, 2005.

[15] I. C. Holm. Multi-pass behaviour of pneumatic tires. *Journal of Terramechanics*, 6(3):47–71, 1969.

[16] Z. Janosi and B. Hanamoto. Analytical determination of drawbar pull as a function of slip for tracked vehicles in deformable soils. In *Proceedings of the 1st International Conference on Terrain-Vehicle Systems*, Turin, Italy, 1961.

[17] L. L. Karafiath and E. A. Nowatzki. *Soil Mechanics For Off-Road Vehicle Engineering*. Trans Tech Publications, Clausthal, Germany, 1978.

[18] T. Koizumi, N. Tsujiuchi, and S. Mori. Simulation of grouser-soil interaction by using 3-dimensional dem considering particle roughness. In *Proceedings of 16th ISTVS International Conference*, pages 221–227, Turin, Italy, 2008.

[19] M. D. Letherwood and D. D. Gunter. Ground vehicle modeling and simulation of military vehicles using high performance computing. *Parallel Computing*, 27:109–140, 2001.

[20] D. Liang, G. Hai-bo, D. Zong, and T. Jian-guo. Wheel slip-sinkage and its prediction model of lunar rover. *J. Cent. South Univ. Technol.*, 17:129–135, 2010.

[21] M. Loo. A model analysis of tire behavior under vertical loading and straight-line free rolling. *Tire Science and Technology*, 13(2):67–90, 1985.

[22] T. Muro and J. O'Brien. *Terramechanics: Land Locomotion Mechanics*. A. A. Balkema Publishers, 2004.

[23] Society of Automotive Engineers. Vehicle dynamics terminology. In *SAE J670e*, Warrendale, PA, 1978.

[24] C. Senatore. *Prediction of mobility, handling, and tractive efficiency of wheeled off-road vehicles*. PhD thesis, Virginia Polytechnic Institute and State University, Blacksburg, VA, 2010.

[25] A. M. Sharaf, G. Mavros, H. Rahnejat, P. D. King, and S. K. Mohan. Optimisation of awd off-road vehicle performance using visco-lock devices. *Int. J. Heavy Vehicle Systems*, 15(2/3/4):188–207, 2008.

[26] A.M. Sharaf, H. Rahnejat, and P.D. King. Analysis of handling characteristics of all-wheel-drive off-road vehicles. *Int. J. Heavy Vehicle Systems*, 15(1):89–106, 2008.

[27] H. Shibly, K. Iagnemma, and S. Dubowsky. An equivalent soil mechanics formulation for rigid wheels in deformable terrain, with application to planetary exploration rovers. *Journal of Terramechanics*, 42:1–13, 2005.

[28] S. Shoop, , I. Darnell, and K. Kestler. Analysis of tire models for rolling on a deformable substrate. *Tire Science and Technology*, 30(3):180–197, July 2002.

[29] S. Shoop, K. Kestler, and R. Haehnel. Finite element modeling of tires on snow. *Tire Science and Technology*, 34(1):2–37, March 2006.

[30] K. Terzaghi, R. B. Peck, and G. Mesri. *Soil Mechanics in Engineering Practice*. John Wiley & Sons, New York, 3rd edition, 1996.

[31] J. Y. Wong. *Theory Of Ground Vehicles*. John Wiley & Sons, New York, 3rd edition, 2001.

[32] J. Y. Wong. *Terramechanics and Off-Road Vehicle Engineering*. Elsevier, UK, 2nd edition, 2010.

[33] J. Y. Wong and A. R. Reece. Prediction of rigid wheel performance based on analysis of soil-wheel stresses, Part I. Performance of driven rigid wheels. *Journal of Terramechanics*, 4(1):81–98, 1967.

[34] J. Y. Wong and A. R. Reece. Prediction of rigid wheel performance based on analysis of soil-wheel stresses, Part II. Performance of towed rigid wheels. *Journal of Terramechanics*, 4(2):7–25, 1967.

[35] J. Yamakawa, A. Kojima, and K. Watanabe. A method of torque control for independent wheel drive vehicles on rough terrain. *Journal of Terramechanics*, 44:371–281, 2007.

[36] Z. Yu, H. Tan, X. Du, and L. Sun. A simple analysis method for contact deformation of rolling tire. *Vehicle System Dynamics*, 36(6):435–443, 2001.

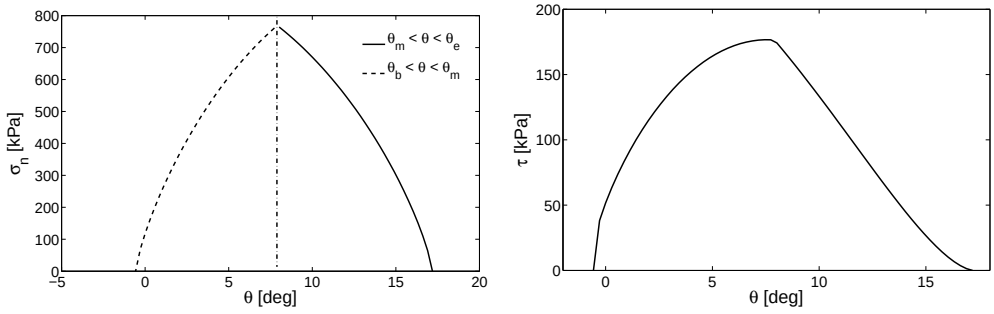

(a) (b)

Figure 1: (a) Normal stress distribution along the contact patch of a driven ($s_d = 0.2$) rigid wheel. The stress increases from the entry angle θ_e, reaches the maximum at θ_m, and decreases back to zero at the exit angle θ_b. (b) Tangential stress distribution along the contact patch under the same assumptions.

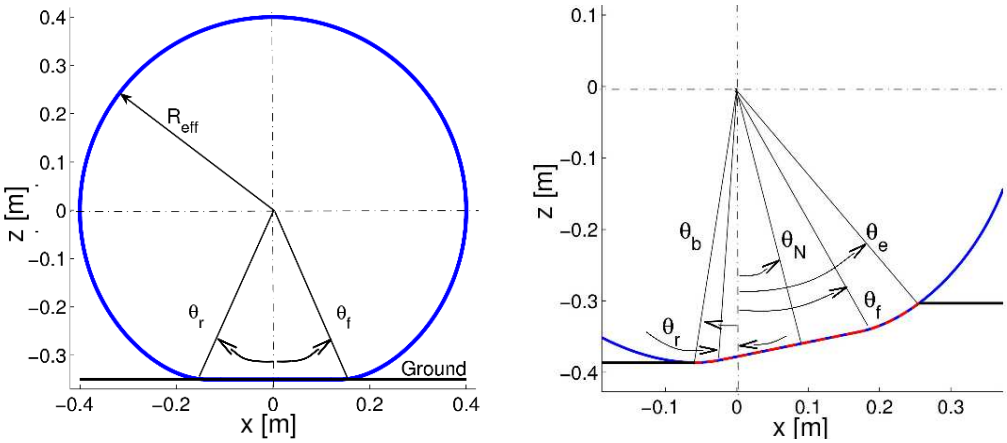

(a) (b)

Figure 2: Exaggerated plot of a deformed tire sitting on hard surface (a) and driven on a soft terrain (b). When stationary the only portion in contact with the terrain is the flat region between θ_r and θ_f which in this particular configuration correspond to θ_b and θ_e. When the tire is rolling, the section of maximum deflection is rotated on an angle $\theta_m = \frac{\theta_f}{2}$ and the entry and exit angle $\theta_{e,b}$ don't necessarily correspond to θ_f and θ_r.

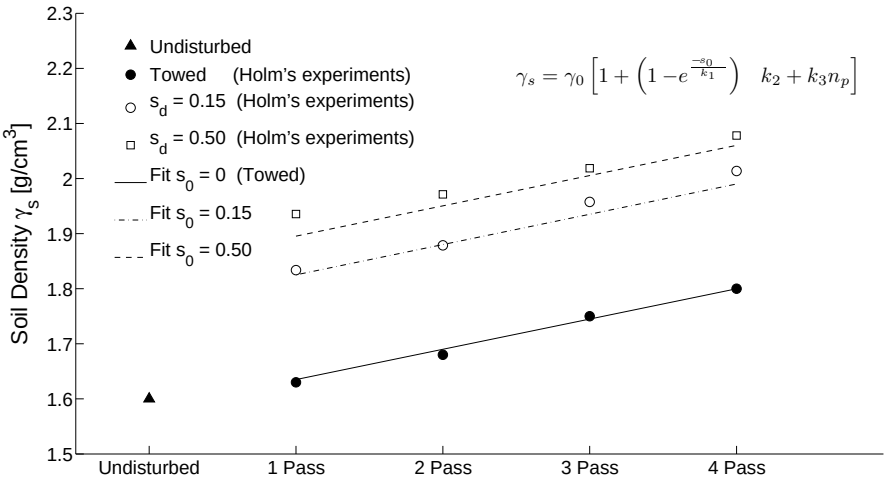

Figure 3: Variation of density recorded by Holm [15] during multipass experiments. Line fit parameters k_1, k_2 and k_3 are the same for every line.

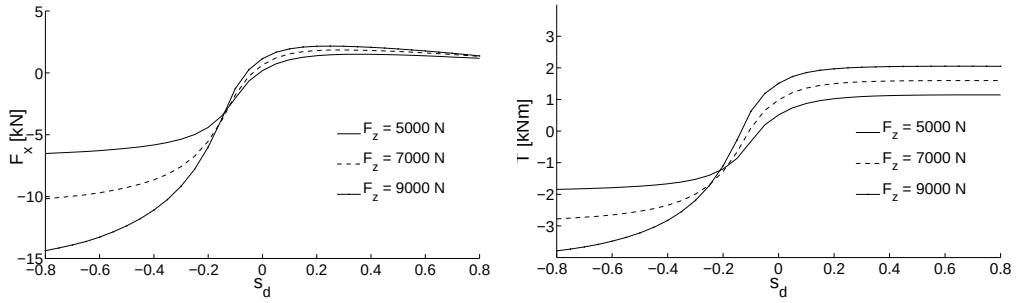

(a) (b)

Figure 4: Trend of drawbar pull (a) and driving torque (b) for different vertical loads and slip ratio. Results obtained for a rigid wheel running on dry sand.

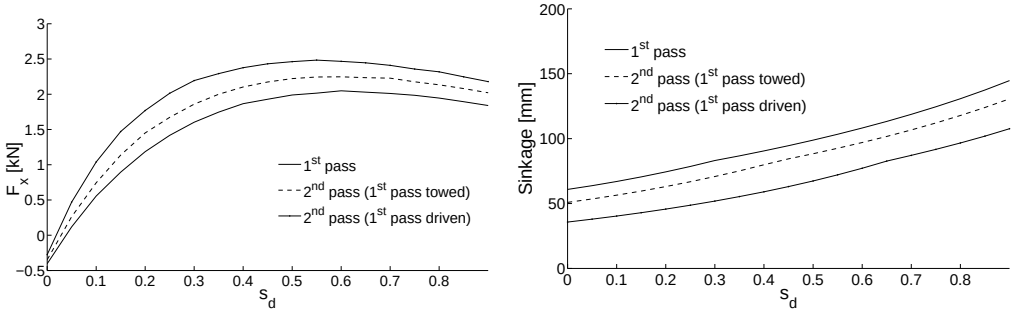

(a) (b)

Figure 5: Multi-pass influence on the performance of rigid wheels on dry sand. In (a) the longitudinal force is presented while (b) shows the relative sinkage.

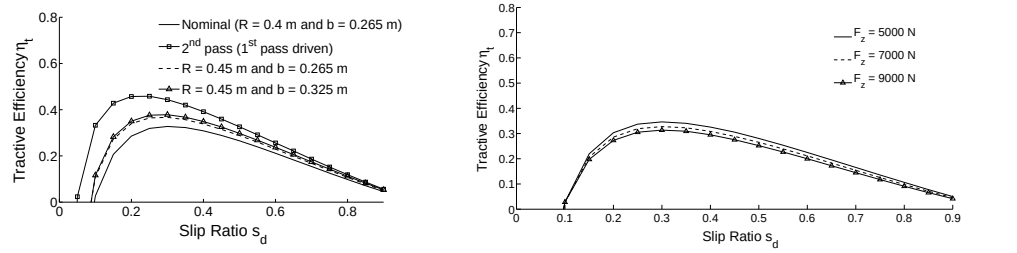

(a) (b)

Figure 6: Tractive efficiency under different operational scenarios for a tire rolling on dry sand. In (a) different sizes and the multi-pass effect influence is showed. In (b) different loads are investigated.

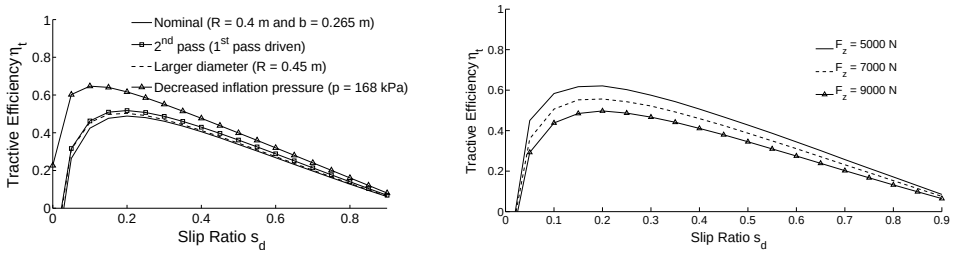

(a) (b)

Figure 7: Tractive efficiency under different operational scenarios for a tire rolling on moist loam. In (a) different inflation pressures, tire sizes, and the multi-pass effect influence is showed. In (b) different loads are investigated.

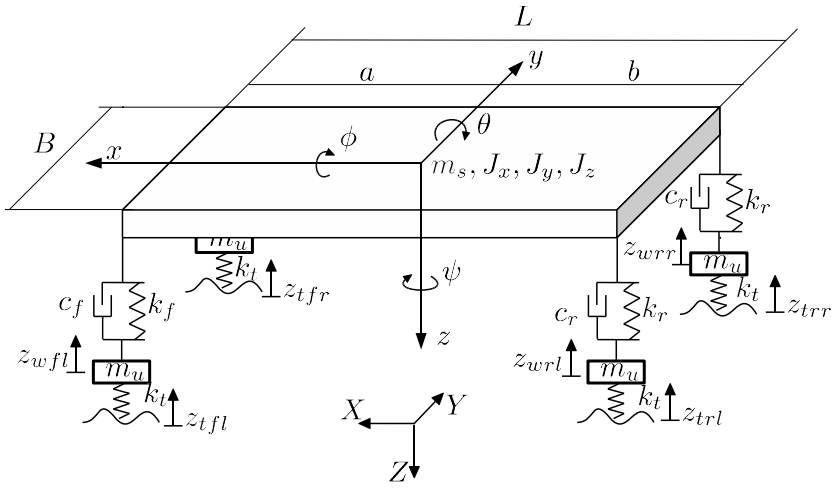

Figure 8: Schematic representation of the vehicle model. The earth-fixed reference frame X,Y,Z is showed and can be arbitrarily located. The vehicle motion is described in terms of the right-handed reference frame x,y,z attached to the vehicle center of gravity. The wheels displacement is constrained in the z-direction of the vehicle-fixed reference frame. To keep the plot clear the x',y',z' frame is not illustrated.

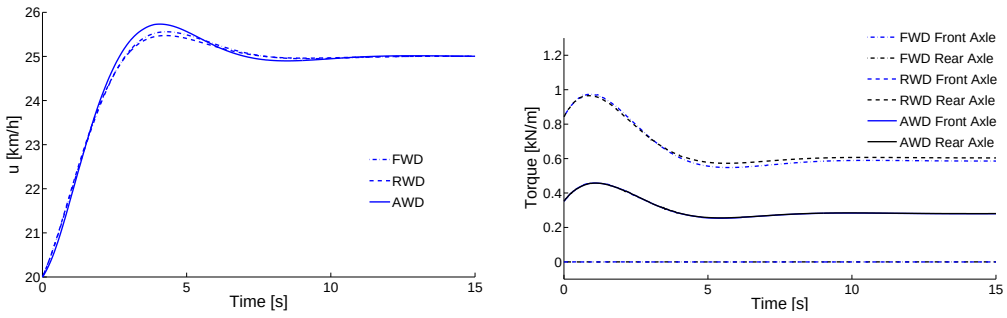

(a) (b)

Figure 9: (a) Velocity profile for a vehicle running on a flat dry sand terrain. The simulation starts from a slightly lower velocity in order to reach smooth steady state conditions. (b) The torque delivered at the tires during the maneuver.

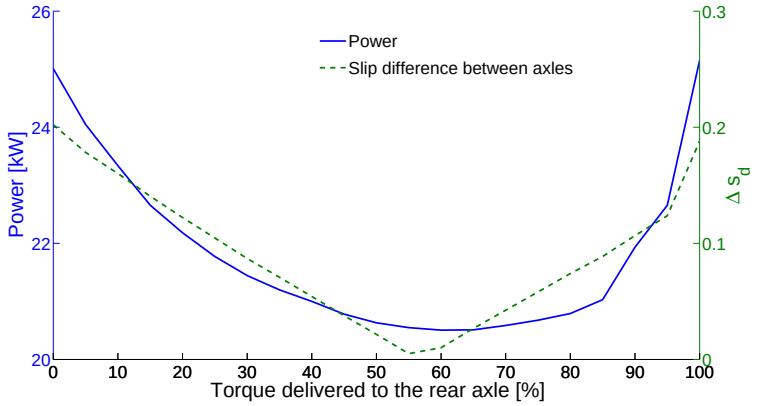

Figure 10: Power vs. torque distribution for a vehicle traveling at 25 km/h on flat dry sand. 0 % (100 %) on the x-axis means that the torque is fully biased on the front (rear) axle of the vehicle. On the same plot slip difference between axles is plotted. Power is not minimized when slip difference is minimized. However, in this particular configuration, the two minima are very close.

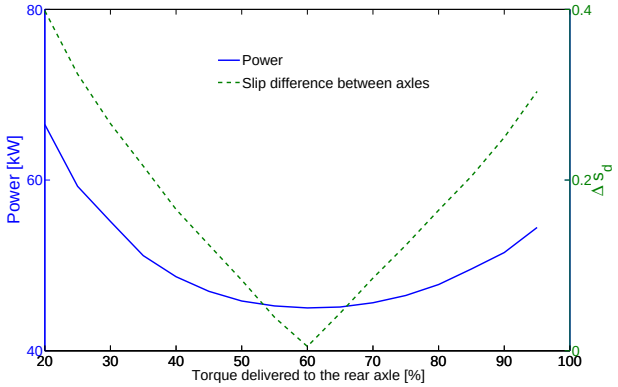

Figure 11: Power vs torque distribution for a vehicle traveling at 25 km/h on a 10 % incline. 0 % (100 %) on the *x*-axis means that the torque is fully biased on the front (rear) axle of the vehicle. Pure RWD and FWD vehicles failed to complete the simulation because they did not have enough traction.

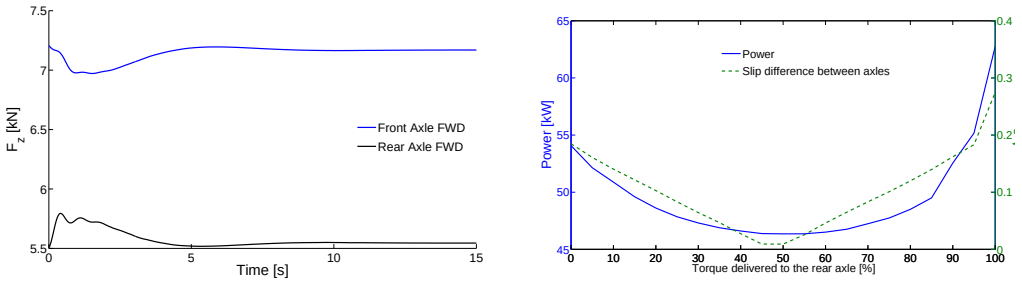

(a) (b)

Figure 12: (a) Vehicle with a significant static load distribution unbalance during a straight run at 50 km/h on dry sand. (b) Power vs torque distribution among the axles.

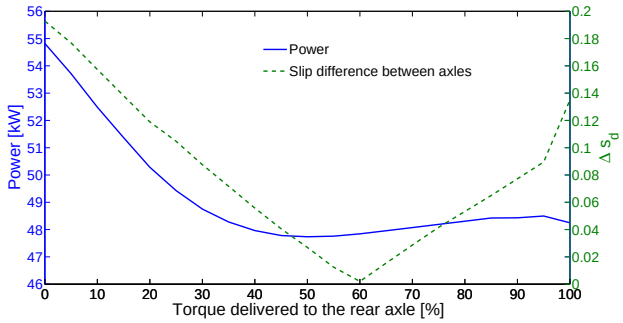

Figure 13: Power vs torque distribution for a vehicle traveling at 50 km/h on flat loam. 0 % (100 %) on the *x*-axis means that the torque is fully biased on the front (rear) axle of the vehicle.

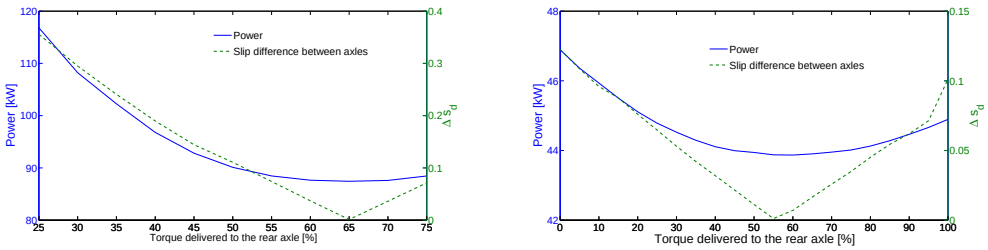

(a) (b)

Figure 14: (a) Torque distribution influence on the performance of an AWD vehicle driving at 50 km/h on a 10% inclined loam terrain. The best efficiency is reached when 60% of the total torque is delivered to the rear axle. (b) Torque distribution influence on the performance of an AWD vehicle driving at 50 km/h on a flat loamy terrain with reduced tire inflation pressure. The best efficiency is reached when 60% of the total torque is delivered to the rear axle.